

## Detection of the entrance of Lugol's solution into the aleurone layer during germination\*\*

Jakub Lev\*, Liubou Kameneva and Jiří Blahovec

Czech University of Life Sciences Prague, Faculty of Engineering, Department of Physics  
Kamýcká 129, 165 00 Prague 6 - Suchbátka, Czech Republic

Received September 14, 2018; accepted March 6, 2019

**Abstract.** The movement of water into dry kernels is a critical step in germination, preharvest sprouting, and in the expression of dormancy. The soaking of kernels in Lugol's solution allows for water uptake visualization by staining the cellular membranes and starch tissue. It is possible to recognize a stained aleurone layer during germination via image analysis (without cutting). A new method for the detection of Lugol's solution in the aleurone layer of four wheat varieties is presented. The first entrance of the solution into the aleurone layer was detected. The rate at which the solution spread through the aleurone layer was also demonstrated. It was determined that the initial entrance time of the solution into the aleurone layer was different for the individual varieties (1.5-6 h) whereas the rate at which it spread in the aleurone layer was similar for the tested varieties and takes approximately  $0.2\text{-}0.35\text{ mm h}^{-1}$ . It was established that there is a close correlation between the solution speed in the aleurone layer and the mass increase during solution uptake for 3 out of 4 varieties.

**Keywords:** imbibition, wheat, image analysis, germination phases, method

### INTRODUCTION

Water uptake and movement in the kernels plays a key role during germination (King, 1984; Bewley, 1997). Water allows for the initiation of important metabolic activities and thus allows the kernel to develop (Kornarzyński *et al.*, 2002; Resio *et al.*, 2006; Weitbrecht *et al.*, 2011; Ünal *et al.*, 2013). That is why the water dynamics of germinating kernels is usually used as a chronological marker in physiological studies focusing on the germination process (Ribeiro-Oliveira and Ranal, 2017). Dong *et al.* (2015) presented a dynamical proteome analysis of wheat kernel

germination. The authors revealed the dynamical changes in the proteome involved in wheat kernel germination. They also showed the connection between the dynamic changes observed in the proteome and the germination phases.

Water movement was monitored using different methods (Kikuchi *et al.*, 2006). One of them consists of monitoring the morphological changes in a kernel using different methods of microscopy, including electron microscopy (Dell 1980; McDonald *et al.*, 1988). Nakanishi and Matsubayashi (1997) used non-destructive water imaging with neutron beam analysis in living plants. Nuclear magnetic resonance imaging or magnetic resonance imaging (MRI) may be used to trace dynamic water movement in plant tissues, including a kernel during its germination (Rokitta *et al.*, 1999; Gruwel *et al.*, 2001; Kikuchi *et al.*, 2006). Gruwel *et al.*, (2001) presented a magnetic resonance study of water uptake in barley kernels. They were able to distinguish between two stages of germination corresponding to two phases of germination. Rathjen *et al.* (2009) used micromagnetic resonance imaging for the detection of water movement during the germination of wheat kernels. These authors, among others, precisely described water distribution during the imbibition phase. The data were collected at hourly intervals from 2 to 18 h. At the beginning (during the initial two hours of imbibition) the water was mainly located between the true kernel coat and the kernel pericarp and also in the micropyle, where the water enters into the kernel. The water did not penetrate across the coat into the endosperm. During the imbibition

\*Corresponding author e-mail: jlev@tf.czu.cz

\*\*This work was supported by the Internal Grant Agency of the Czech University of Life Sciences Prague, Project No. 31120/1312/3110 (2017).

process, the water hydrated the entire embryo. After this stage, water began to penetrate into the endosperm through the scutellum.

Water produces strong absorption bands in the near infrared (NIR) region (Govender *et al.*, 2007) and this may be used to determine moisture content or more simply for water detection in the germinated grain (Manley *et al.*, 2011). In this study, a combination of near infrared hyperspectral imaging and chemometrics was used for the study of water diffusion in wheat kernels with different hardness values. Deionised water (dH<sub>2</sub>O) and deuterium oxide (D<sub>2</sub>O) were used for this purpose. Lancelot *et al.* (2017) used near infrared hyperspectral imaging for monitoring water diffusion in wheat kernel sections. These authors reported that their system allows for the real-time monitoring of water diffusion into different tissues of the wheat kernels and that it may be fully automated. However, they also presented several limitations of this system.

The most frequent method used for water diffusion monitoring in kernels is based on iodine staining (Kikuchi *et al.*, 2006). Rathjen *et al.* (2009) demonstrated that Lugol's solution (I<sub>2</sub>/KI) was found to be the most effective marker for visualizing water uptake into the kernel tissue. However, the disadvantage of this method is that the kernels are cut at the evaluation stage.

Individual kernel parts have different colours after iodine staining. Whereas the embryo and the kernel coat have a relatively light brown colour, the endosperm, including the aleurone layer is almost black (Rathjen *et al.*, 2009; Lev and Blahovec, 2018). The colouring of the aleurone layer and the endosperm is so intensive that the level of its darkness can be detected through the kernel coat. This technique is used in this paper with the aim of studying the water pathway in the aleurone layers of the tested kernels.

#### MATERIALS AND METHODS

Four varieties of winter wheat (*Triticum aestivum* L.) were used in the experiment: Tosca, Steffi, Turandot and Vanesa (supplier: Selgen Plc.) and the weights of 1000 kernels of each variety were 46.4, 50.5, 52.3, and 52.9 g, respectively. The wheat varieties were harvested in 2016 and the grains used in the experiment were stored in a laboratory. Their moisture contents before the experiment (wet basis) were determined to be 6-7% (ASABE Standard S358.2, 2006).

Imbibition monitoring was performed on three layers of a polyester cloth (white Novolin, area density: 100 g m<sup>-2</sup>). The polyester cloths and the kernels were placed into a glass vessel and the cloth was moisturised by 12 g of I<sub>2</sub>/KI water solution. The I<sub>2</sub>/KI solution contained: 1 g I<sub>2</sub>, 2.5 g KI and 96.5 ml distilled water. In an attempt to minimize water evaporation, the glass vessel was covered by a thin glass plate. One simple experiment consisted of monitoring six kernels from each variety i.e. 24 kernels. This experiment was replicated seven times so that for each variety 42 kernels were monitored.

The laboratory setup (Fig. 1) consisted of a still camera (Canon EOS 750D with lens Canon 18 55 mm) (2), a stand (1), a bottom illumination LED panel (neutral white, 6000 K) (5), an upper LED light (neutral white, 4000 K) (3) and a glass vessel with the monitored kernels (4).

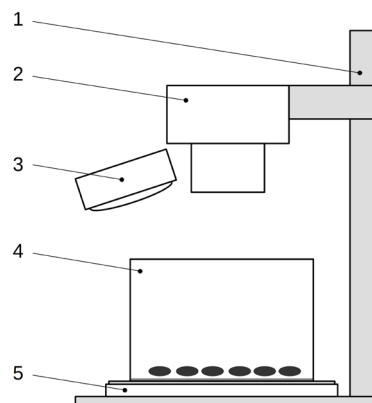


**Fig. 1.** The schema of the laboratory setup. 1 – stand, 2 – camera, 3 – upper LED light, 4 – glass vessel, 5 – bottom illumination LED panel.

The laboratory setup was placed in an incubator (Friocell 111 EVO, manufacturer: BMT Medical Technology Inc.) which ensured a constant temperature 21°C during the whole experiment. The air pressure ranged between 98.0 and 99.5 kPa. The camera and the LED lights were controlled *via* computer using a program written in the Python programming language (<https://www.python.org>, version 2.7). The focal length was set to view the top surface of the kernels. Every two minutes two photographs with different light schemes were taken. For the first one the CI (the “contrast image”) was taken with the bottom light only. This allowed for the easy detection of the individual kernels (reaching the highest possible contrast between the kernels and the background). For the second photo both the bottom and the upper lights were used together (this photo was denoted as a “light image”, LI for short). The LI made it possible to detect changes on the top surface of the kernels. One test took 24 h: during this period 2 × 720 photographs of the 24 kernels tested were collected. Each kernel was weighed before and after the test with the aim of determining the mass increase of the kernel ( $\Delta m$ ). Scale used: Kern EW120 – 4NM (accuracy: 0.001 g).

The detection of the outlines of the individual kernels were carried out using the CI. The images were converted to the grey scale (green channel). We noted a moderate brightness increase in the background during the test, therefore we converted the images according to the following formula:

$$f_c(x, y) = \frac{f(x, y)C}{B}$$

where:  $f_c(x, y)$  is the converted image, and  $f(x, y)$  is the original image. The parameters  $C$  and  $B$  are the brightness values of the CI backgrounds ( $C$  is the preferred basic value and  $B$  represents the real observed value). This procedure allows

for a precise detection of the kernel outlines regardless of the increase in brightness. Then the image was converted into a binary image and an erosion-dilation filter for noise reduction was applied (Gonzalez and Woods, 2002). The detected outlines were used for the selection of the kernel regions in the LI (the position of the kernels is identical in both images LI and CI). These regions were then rotated so that its major axis was parallel to the  $x$ -axis (Gonzalez and Woods, 2002; Lev and Blahovec, 2017). The kernel regions were converted to the grey scale. The red channel was used because it was found to be the most sensitive one in the detection of iodine colouring.

Two strips were selected from the regions of the kernel. The widths of both strips were  $0.15 L$ , where  $L$  is the kernel length. The first strip was located  $0.2 L$  from the left edge of the kernel (which is formed by the kernel embryo) and the second strip was located  $0.5 L$  from the same side of the kernel (see Fig. 2.). The region of the first strip includes a boundary around the internal side of the embryo: the first indicators of  $I_2/KI$  solution infiltration to the aleurone layer should be visible in this region (Rathjen *et al.*, 2009). The mean values of brightness were calculated for both strips and the values were stored in a log file.

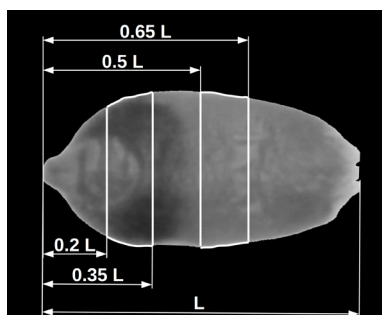


**Fig. 2.** The kernel region from LI (light image) after converting to the grey scale. The strips used for analysis are marked in white. The dark colouring on the left side indicates the  $I_2/KI$  presence in the aleurone layer.

The time developments of brightness contain several characteristic break points. These points may be mathematically described as local extrema of the curve's second derivative. The time derivatives were calculated numerically (Lev *et al.*, 2017). The data was sequentially fitted (the fitted interval contains 60 points for the first strip and 120 points for the second strip) by straight lines and the straight lines parameters were determined through the application of the least squares method. The slopes of the straight lines are understood to be a local derivative of the plot.

Image processing and data analysis were performed by the Python 3.4 programming language (<https://www.python.org>) and by its supporting libraries: OpenCV 3.4.0, NumPy 1.14.1, SciPy 1.1.0 and Matplotlib 1.3.1. The varieties were compared using the Kruskal-Wallis test and Dunn's test (Dunn, 1964) (software R, <https://www.r-project.org>, version 3.0.2).

## RESULTS AND DISCUSSION

An example of an experimental result is given in Fig. 3: it includes a time course of the mean brightness of the monitored strips for one of the tested kernels. The curve developments relate to the presence and location of the  $I_2/KI$  solution in the observed region. The time courses of the brightness in Fig. 3 contain three break points ( $P_0$ ,  $P_1$  and  $P_2$ ) that divide the brightness curve into four characteristic stages. The graphs also include grey denoted curves that represent the second derivatives of the initial dependences; these curves were used for the determination of the characteristic points:  $P_0$ ,  $P_1$  and  $P_2$ .

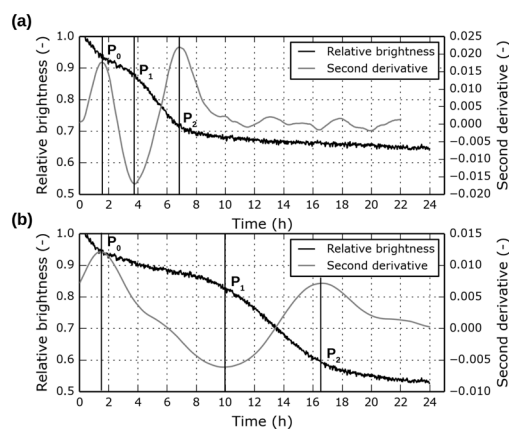


**Fig. 3.** Time progress of relative mean brightness in the monitored strips in the kernel regions; the characteristic points  $P_0$ ,  $P_1$  and  $P_2$  correspond to the extreme points of the second derivative time plots, for details see text (a) the data for the first strip (near to embryo part). The point  $P_1$  indicates the first entrance of  $I_2/KI$  into the aleurone layer ( $T_1$ ), (b) the data for the second strip.

The first stage, prior to point  $P_0$ , is relatively short (approximately 1-2 h in most cases) and it is characterized by a decrease in brightness. This decrease is caused by  $I_2/KI$  presence in the kernel coat (between the true coat and the pericarp) which then becomes stained by the brown colour. The rate of brightness decrease slows down in the second stage between points  $P_0$  and  $P_1$ . This is caused by the coat saturation of the  $I_2/KI$  solution. In the third stage (between  $P_1$  and  $P_2$ ) a significant decrease in brightness, is again observed. The  $I_2/KI$  solution enters the aleurone layer in the monitored area (strip) and stains it a dark colour. The beginning of the third stage (point  $P_1$ ) is different for the first and second strips. The first strip is in the area where the  $I_2/KI$  solution should enter the aleurone layer first and therefore  $P_1$  may represent this event. It is known that water progresses from the embryo to the brush during imbibition (Rathjen *et al.*, 2009). This is consistent with our observations and it explains why point  $P_1$  occurs later in the case of the second strip. The third stage is terminated by  $P_2$ : this point indicates that most of the monitored region is stained. In the fourth and final stage (at a time after  $P_2$ ), only a slight decrease in brightness was detected.

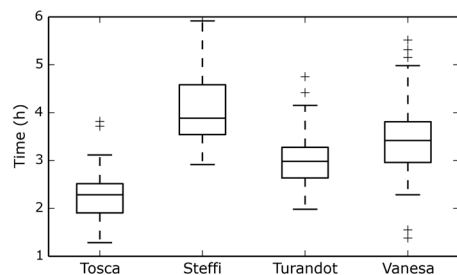


**Fig. 4.** Time of the first entrance of  $I_2/KI$  into the aleurone layer ( $T_1$ ) for different varieties. Mean values, interquartile range, outside values and outliers are depicted in the box-plots.

In further discussion we will concentrate on two characteristic points:  $P_1$  in the first strip and  $P_2$  in the second strip (see Fig. 3). The first one may be understood as an initiation of the liquid motion into the aleurone layer, whereas the second one corresponds to the final part of this process. The first point also represents the first entrance of  $I_2/KI$  into the aleurone layer ( $T_1$ ) and it may correspond to the entrance of  $I_2/KI$  into the endosperm, as well. Fig. 4 includes  $T_1$ -values obtained for different varieties:  $T_1$  varies from 1.5 to 6 h. The lowest values were found for Tosca (the average value was a little higher than 2 h) and the highest values were found for Steffi (average value ca. 4 h).

The  $T_1$  values for different varieties were compared using the Kruskal-Wallis test and Dunn's test. Statistically significant differences were found among the tested varieties except for Vanesa and Turandot (p-value 0.136). For the other combinations the p-values were lower than 0.01.

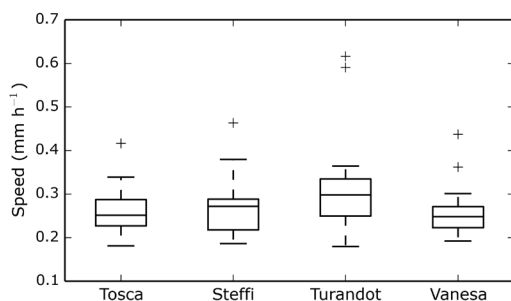


**Fig. 5.** Speed of  $I_2/KI$  movement in the aleurone layer for different varieties. Mean values, interquartile range, outside values and outliers are depicted in the box-plot.

The time differences between point  $P_1$  of the first strip and point  $P_2$  of the second strip together with the known distance between the monitored strips may be used to

estimate the speed of the  $I_2/KI$  movement in the aleurone layer. This speed ( $V$ ) is depicted in Fig. 5. The value of  $V$  is similar for all tested varieties and it varies in the range 0.2–0.35  $\text{mm h}^{-1}$ . The Kruskal-Wallis test and Dunn's test for  $V$  did not show any significant differences between the tested varieties. Figure 6 includes the relative mass increase ( $\Delta m$ ) of kernels during the measurement (24 h). The highest values of  $\Delta m$  were observed for the Tosca variety and the lowest ones for the Turandot variety. The differences are relatively small. However, significant differences were not only observed between Tosca and Steffi (p-value 0.09) they also occur between Turandot and Vanesa (p-value 0.377).

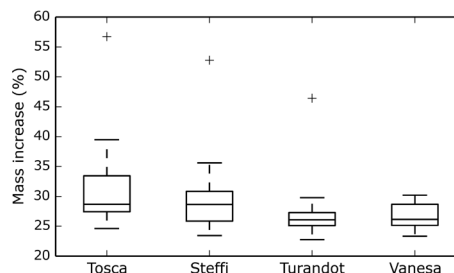


**Fig. 6.** The mass increase during water uptake for different varieties. Mean values, interquartile range, outside values and outliers are depicted in the box-plot.

The mutual relationship between  $T_1$ ,  $V$  and  $\Delta m$  were assessed by Pearson's correlation coefficient. The correlation was calculated for all of the varieties together and also for the individual varieties. The correlation coefficients together with the p-values are shown in Table 1. Small or moderate correlations were mainly found between  $T_1$  and  $V$ . A significant correlation was only found for the Steffi variety. The negative coefficient ( $R = -0.558$ ) indicates an indirect proportionality between  $T_1$  and  $V$ . A slightly better correlation but still mainly a small or moderate one was found between  $T_1$  and  $\Delta m$ . With the exception of the Tosca variety these correlations were significant. The negative coefficients indicate that a more rapid penetration of the solution through the embryo relates to the higher final moisture content. Close or even very close and significant correlations were found between  $V$  and  $\Delta m$ . They show that the amount of the solution absorbed during the measurement primarily depends on  $V$ . An exception to this rule is the Vanesa variety for which the correlation coefficient was only -0.067.

**Table 1.** Mutual relations between  $T_1$ ,  $V$ ,  $\Delta m$  assessed by Pearson's correlation coefficient

Varieties	$T_1 \sim V$		$T_1 \sim \Delta m$		$V \sim \Delta m$	
	correlation coefficient	p-value	correlation coefficient	p-value	correlation coefficient	p-value
All varieties	-0.178	0.051	-0.29 *	0.001	0.557 *	< 0.001
Tosca	-0.282	0.131	-0.165	0.385	0.863 *	< 0.001
Steffi	-0.558 *	0.001	-0.380 *	0.038	0.719 *	< 0.001
Turandot	-0.304	0.103	-0.375 *	0.041	0.687 *	< 0.001
Vanesa	0.149	0.434	-0.463 *	0.01	-0.067	0.725

\* indicates significant correlation (p-value < 0.05).

The performance of the experiments required only minimum intervention. After the preparation of the specimens, the only requirement was to set several parameters for image analysis. The values of the parameters were checked during every measurement, but the same parameters were used in all cases. It may be concluded that the whole process of data evaluation is suitable for full automation from a practical point of view.

The time development of brightness (Fig. 3) indicates only minor fluctuations and points  $P_0$ ,  $P_1$  and  $P_2$  are clearly noticeable. Only in a few cases (up to 5%) were less pronounced curve breaks noted and thus the detection of the break points was more difficult. These complications seem to be caused by the kernel coat which reduced the visibility of the darker aleurone layer.

Phase I of the three step germination process (Bawley, 1997; Weitbrecht *et al.*, 2011) takes about 5-7 hours (Abenavoli *et al.*, 2006; Dell'Aquila, 2006; Rathjen *et al.*, 2009; Harb, 2013). Our results for the lowest characteristic time  $T_1$  for the entrance of the solution into the aleurone layer is much lower (Fig. 4), in the case of Tosca it was only 2.3 h. That is why an additional experiment was performed. The kernels (Tosca variety) were soaked in the solution for the time intervals of 0.5, 1, 3, 5 h. Then the samples were bisected longitudinally through the crease with a blade and images of the inward side were taken to detect if the solution reached the aleurone layer. A bisected kernel after 3 h of soaking in the solution is shown in Fig. 7. On the left side of the figure, the whole embryo including the scutellum is visible. The solution has reached the aleurone layer next to the embryo where it can be detected by our method. Similar results were observed in other samples. The results of this measurement showed that in one case the solution had already reached the aleurone layer after 1 h. After 3 h the position of the solution was visible in 18 cases out of 20, and after 5 h the solution had reached the aleurone layer in all cases. This observation is in agreement with the results shown in the Fig 4.



**Fig. 7.** Example of a kernel bisected longitudinally through the crease after 3 h of imbibition (variety Tosca).

Fig. 7 also indicates the path of solution propagation. A significant amount of the solution went around the embryo. In the example shown in Fig. 7 it is visible, espe-

cially around the upper part of the embryo. Also, it may be seen that the solution reached the upper part of the scutellum first and then continued into the aleurone layer.

Parameter  $T_1$  varied between the tested varieties. In order to discover the cause, Pearson's correlation coefficients were calculated between  $T_1$  and other known parameters (size, surface area projections, and weight). However, only loose correlations were found. Therefore, the probable cause of this behaviour could be the differences in the kernel and embryo structure and the different penetrability of these materials by the solution.

The parameter  $V$  reveals further information concerning the imbibition process. Compared to  $T_1$ , this parameter reaches similar values for different varieties. This indicates that the diffusion properties of the aleurone layer are similar for different varieties. It is not surprising that the parameter  $V$  corresponds to  $\Delta m$  in the correlation table (Table 1 – see the close or very close correlations between  $V$  and  $\Delta m$  for Tosca, Steffi and Turandot). However, almost zero correlation was found in the case of the Vanesa variety which indicates that the relationship may be more complicated in some cases. Certainly, the properties of the endosperm also plays some role in this process.

## CONCLUSIONS

1. The presented method allows for the detection of water solution  $I_2/KI$  movement in the aleurone layer using a non-invasive method. The whole process was fully automated.
2. In the presented paper, we detected an event that should correspond with the first entrance of the solution into the aleurone layer and we also determined its speed in the aleurone layer. Whereas, the first entrance time of the solution into the aleurone layer is different for individual varieties (1.5-6 h), the solution speed in the aleurone layer is similar in the tested varieties and falls into the approximate range of 0.2-0.35 mm h<sup>-1</sup>. Close and very close correlations (0.687-0.863) were found between the solution speed in the aleurone layer and the mass increase for 3 out of 4 varieties.

**Conflict of interest:** The authors declare that they have no conflict of interest.

**Compliance with ethical requirements:** This study does not contain any experiment involving human or animal subjects.

## REFERENCES

- Abenavoli M.R., Cacco G., Sorgonà A., Marabottini R., Paolacci A.R., Ciaffi M., and Badiani M., 2006. The inhibitory effects of coumarin in the germination of durum wheat (*Triticum turgidum* ssp. durum, CV. Simeto) seeds. J. Chem. Ecol., 32, 489-506. <https://doi.org/10.1007/s10886-005-9011-x>
- ASABE Standards, 2006. S358.2 Moisture measurement-Forages. St. Joseph, Michigan, USA.

- Bewley J.D., 1997.** Seed germination and dormancy, *Plant Cell*, 9, 1055-1066. <https://doi.org/10.1105/tpc.9.7.1055>
- Dell'Aquila A.D., 2006.** Computerized seed imaging: a new tool to evaluate germination quality. *Communications in Biometry Crop Sci.*, 1, 20-31.
- Dell B., 1980.** Structure and function of the strophilar plug in seeds of *Albizia lophantha*. *Am. J. Bot.*, 67, 556-563. <https://doi.org/10.1002/j.1537-2197.1980.tb07684.x>
- Dong K., Zhen S., Cheng Z., Cao H., Ge P., and Yan Y., 2015.** Proteomic analysis reveals key proteins and phosphoproteins upon seed germination of wheat (*Triticum aestivum* L.). *Front. Plant Sci.*, 6, 1-14. <https://doi.org/10.3389/fpls.2015.01017>
- Dunn O.J., 1964.** Multiple comparisons using rank sums. *Technometrics*, 6, 241-252. <https://doi.org/10.1080/00401706.1964.10490181>
- Gonzalez R.C. and Woods R.E., 2002.** Digital Image Processing. Prentice Hall, New Jersey, USA.
- Govender M., Chetty K., and Bulcock H., 2007.** A review of hyperspectral remote sensing and its application in vegetation and water resource studies. *Water SA*, 33, 145-152. <https://doi.org/10.4314/wsa.v33i2.49049>
- Gruwel M.L.H., Chatson B., Yin X.S., and Abrams S., 2001.** A magnetic resonance study of water uptake in whole barley kernels. *Int. J. Food Sci. Technol.*, 36, 161-168. <https://doi.org/10.1046/j.1365-2621.2001.00445.x>
- Harb A.M., 2013.** Reserve mobilization, total sugars and proteins in germinating seeds of durum wheat (*Triticum durum* Desf.) under water deficit after short period of imbibition. *Jordan J. Biological Sci.*, 6, 67-72. <https://doi.org/10.12816/0000261>
- Kikuchi K., Koizumi M., Ishida N., and Kano H., 2006.** Water uptake by dry beans observed by micro-magnetic resonance. *Imaging Annals of Botany*, 98, 545-553. <https://doi.org/10.1093/aob/mcl145>
- King R.W., 1984.** Water uptake in relation to pre-harvest sprouting damage in wheat: grain characteristics. *Aust. J. Agr. Res.*, 35, 337 - 345. <https://doi.org/10.1071/AR9840337>
- Kornarzynski K., Pietruszewski S., and Lacek R., 2002.** Measurement of the water absorption rate in wheat grain. *Int. Agrophys.*, 16, 33-36.
- Lancelot E., Bertrand D., Hanafi M., and Jaillais B., 2017.** Near-infrared hyperspectral imaging for following imbibition of single wheat kernel sections. *Vib. Spectrosc.*, 92, 46-53. <https://doi.org/10.1016/j.vibspec.2017.05.001>
- Lev J., Křepčík V., Prošek V., and Kumbála F., 2017.** Capacitive throughput sensor for plant materials - Effects of frequency and moisture content. *Computers Electronics Agric.*, 133, 22-29. <https://doi.org/10.1016/j.compag.2016.12.014>
- Lev J., and Blahovec J., 2017.** Imbibition of wheat seeds: Application of image analysis. *Int. Agrophys.*, 31, 475-481. <https://doi.org/10.1515/intag-2016-0072>
- Lev J., and Blahovec J., 2018.** Effect of I2/KI water solution to wheat seeds imbibition assessed by image analysis. *Agronomy Research*, 16, 492-499.
- Manley M., du Toit G., and Geladi P., 2011.** Tracking diffusion of conditioning water in single wheat kernels of different hardnesses by near infrared hyperspectral imaging. *Analytica Chimica Acta*, 686, 64-75. <https://doi.org/10.1016/j.aca.2010.11.042>
- McDonald M.B., Vertucci C.W., and Roos E.E., 1988.** Seed coat regulation of soybean seed imbibition. *Crop Sci.*, 28, 987-992. <https://doi.org/10.2135/cropsci1988.0011183X002800060025x>
- Nakanishi T.M. and Matsubayashi M., 1997.** Water imaging of seeds by neutron beam. *Bioimages*, 5, 45-48.
- Rathjen J.R., Strounina E.V., and Mares D.J., 2009.** Water movement into dormant and non-dormant wheat (*Triticum aestivum* L.) grains. *J. Exp. Botany*, 60, 1619-1631. <https://doi.org/10.1093/jxb/erp037>
- Resio A.C., Aguerre R.J., and Suarez C., 2006.** Hydration kinetics of amaranth grain. *Food Eng.*, 72, 247-253. <https://doi.org/10.1016/j.jfoodeng.2004.12.003>
- Ribeiro-Oliveira J.P. and Ranal M.A., 2017.** Sample size and water dynamics on germinating diaspores: the first step for physiological and molecular studies on the germination process. *Plant Biosyst.*, 152, 840-847. <https://doi.org/10.1080/11263504.2017.1353551>
- Rokitta M., Zimmermann U., and Haase A., 1999.** Fast NMR flow measurements in plants using FLASH imaging. *J. Magn. Reson.*, 137, 29-32. <https://doi.org/10.1006/jmre.1998.1611>
- Ünal H., Alpsoy H.C., and Ayhan A., 2013.** Effect of the moisture content on the physical properties of bitter melon seed. *Int. Agrophys.*, 27, 455-461. <https://doi.org/10.2478/intag-2013-0016>
- Weitbrecht K., Müller K., and Leubner-Metzger G., 2011.** First off the mark: early seed germination. *J. Exp. Botany*, 62, 3289-3309. <https://doi.org/10.1093/jxb/err030>